Proceedings of ASME Turbo Expo 2023
Turbomachinery Technical Conference and Exposition
GT2023
June 26-30, 2023, Boston, Massachusetts

GT2023-102296

NONLINEAR RESPONSE OF THE ROTOR SUPPORTED BY GAS JOURNAL BEARINGS CONSIDERING STATIONARY AND ROTATING HERRINGBONE GROOVES

Roman Kochurov
SoftInWay, Inc.
Burlington, MA

Leonid Moroz
SoftInWay, Inc.
Burlington, MA

Volodymyr Martynenko
SoftInWay Switzerland GmbH
Zug, Switzerland

ABSTRACT

This paper presents an approach to determine the stability of the rotor in herringbone groove gas journal bearings (HGGJB) based on nonlinear transient analysis. The approach considers rotating (on a rotor) or stationary (on a bearing shell) grooves. The bearing gas film model is described by the Reynolds equations. The finite element (FE) method has been applied to obtain an accurate solution for the HGGJB design. The rotor model is discretized with Timoshenko beam finite elements.

A study on the stability of a rotary machine supported by HGGJBs is performed to investigate threshold rotating speeds for the cases of stationary and rotating grooves applying a nonlinear transient analysis procedure. As a result, the influence of rotating grooves on system stability improvement has been investigated. Additionally, the correspondence of the calculated results to the experimental data available in publications and the nonlinear effects presented on Waterfall plots are also discussed in the article.

The presented method is an extension of previously developed techniques that engineers can use for design and calculation purposes. The nonlinear approach allows accurate simulation of coupled rotor-HGGJB systems and has no limitation for designs with a small number of grooves, as the FE method is used for bearings discretization. The method allows the physical effects of rotating/stationary grooves to be accounted for.

Keywords: herringbone grooved bearing; rotating groove; stationary groove; nonlinear rotor dynamics; stability

1. INTRODUCTION

During the middle of the 20th century, inclined groove patterns were suggested to increase self-acting bearings' pumping capabilities and stability[1]. Building on this concept, herringbone groove gas journal bearings (HGGJBs) have been gaining popularity as supports for lightweight rotors.

A mathematical apparatus has even been developed in recent decades to predict the operation of rotors installed in these bearings. The performance of a gas-lubricated bearing can be described by characteristics such as load capacity, minimal gas film thickness, friction power losses, and flow rate. Stiffness and damping coefficients of the bearing are required for the rotor-bearing system dynamics analysis. These performance characteristics are calculated based on the pressure distribution in the gas film, which is determined as a result of the solution of the Reynolds equation. To solve the Reynolds equation, a 2nd-order nonlinear differential equation, the discretization of the fluid domain must be done, and an appropriate grid is required to describe a herringbone groove geometry precisely. Several discretization methods have been developed to solve the Reynolds equation, such as narrow groove theory (NGT), finite difference method (FDM), finite element methods (FEM), and others.

Early paper studies considering the dynamics of rotors in HGGJBs began to emerge in the middle of the 20th century. The 2D NGT suggested in [2] for dense herringbone patterns could model HGGJBs in a wide operational and parametric range. According to the NGT, the effect of groove number on the bearing characteristics is neglected, and the pressure over the grooves and ridges in the circumferential direction is approximated using linear functions. Many researchers confirmed the approach's effectiveness and accuracy [3,4]. Particularly, the theoretical study [5] where the comparison between NGT, FDM, and CFD was performed also reports a small influence of a finite number of grooves when the number of grooves is comparatively high. However, the NGT has a limitation for designs with a small number of grooves which cuts a significant number of designs as a smaller number of grooves is desirable to reduce manufacturing cost. Bonneau and Absi [6] showed that NGT substantially differs from the load performance of bearings with less than 16 grooves.

The applications of finite difference and finite element methods for HGGJB were extensively developed during the second half of the 20th century to discretize the gas film domain in herringbone groove journal bearings [6,7]. Zirkelback and San Andres [7] applied the finite element method to predict the load and dynamic force coefficients of an HGGJB more accurately and reported a significant improvement over the NGT, especially at high journal eccentricities. Thus, the finite element method gained popularity in this application since it provided the possibility of accurate representation of bearing grooves and lands by inclined finite elements, which can be an advantage for HGGJB designs with a relatively small number of grooves or high journal eccentricities.

Another essential factor is rotor stability which was studied using the linear and nonlinear rotor dynamics models considering stationary and rotating grooves [8–13]. Such studies show that consideration of the rotating domain is crucial as it influences performance parameters and improves the stability of the system [13].

Experimental studies for rotors in herringbone groove journal bearings to ensure HGGJB load capacity, rotor-bearing system stability, and to check the limitations of theoretical results in a wide range of parameters have been performed in [14,15].

More comprehensive investigations took place in HGGJB design. Many studies searched for the optimum bearing parameters [4,13,16], especially in herringbone groove patterns [17,18].

Herringbone groove gas journal bearings have several advantages compared to other types of bearings. They do not require an oil lubrication system compared to hydrodynamic [19] and hydrostatic journal bearings [20]. If properly designed, HGGJBs are not exposed to wear, as with rolling element bearings [21]. Finally, HGGJBs do not require a complex electrical hardware and control system in contrast with active magnetic bearings [22,23].

Therefore, herringbone groove bearing investigations are split in many directions, especially in the field of nonlinear dynamics of the rotor installed in these bearings. Although the difference in nonlinear rotor response in the case of the grooved rotor and grooved journal is insufficiently described in the literature, a detailed comparison of these cases still benefits our understanding of the behavior of genuine rotors in HGGJBs.

The approach for rotor-HGGJB system nonlinear analysis has been developed in the current article. The advantage of the approach is a combination of the finite element method and the option for rotating/stationary groove considerations.

The FE method has no limitations related to the designs (density of groove patterns) of HGGJBs and is currently the most accurate way for continuous system discretization. Whereas consideration of rotating/stationary grooves is necessary to simulate the physics of the rotor-HGGJB system, the performed study presented in the article and comparison with experimental data confirms the significant influence of rotating/stationary grooves on the stability of the system.

2. ANALYSIS METHOD DESCRIPTION

The compressible Reynolds equations in polar coordinates for the modeling of gas herringbone grooved bearings have the following form [24]:

$$\frac{\partial}{R\partial\theta}\left(\frac{ph^3}{12\mu}\frac{\partial p}{R\partial\theta}\right)+\frac{\partial}{\partial z}\left(\frac{ph^3}{12\mu}\frac{\partial p}{\partial z}\right)=\frac{u}{2}\frac{\partial(ph)}{R\partial\theta}+\frac{\partial(ph)}{\partial t} \quad (1)$$

where z, θ, t are axial, circumferential, and time variables; p, h are the pressure and thickness of the gas film; μ is the gas viscosity; $u = \Omega R$ is the sliding velocity of the rotating surface; Ω is the rotor angular velocity; R is the bearing radius.

The viscosity of gases varies little with pressure [25] and is considered constant throughout the bearing:

$$\mu = \mu_0 = \text{constant} \quad (2)$$

The perfect gas model is considered:

$$\frac{p}{\rho} = \overline{R}T \quad (3)$$

where ρ is the gas density; $\overline{R}$ is the gas constant (universal gas constant/molecular weight; T is the gas temperature.

The isothermal model is used since gas bearings normally operate isothermally [25], which means the following:

$$\frac{p}{\rho} = \text{constant} \quad (4)$$

The film thickness is expressed in the form:

$$h = c_g + c + e\cos(\theta - \Phi),$$
$$e = \sqrt{e_x^2 + e_y^2}, \Phi = \arctan\left(\frac{e_y}{e_x}\right) \quad (5)$$

where c_g is groove depth in the groove region or zero in the ridge region; c is the bearing clearance; e, Φ are the eccentricity and the attitude angle; e_x, e_y are the eccentricity components in the x and y directions.

Depending on whether the grooves are stationary or rotating (in other words, if the grooves are on the journal or the shaft), the proper direction and sign of the circumferential coordinate are specified for the model.

The rotor dynamics transient response is simulated based on a complete system of dynamic equations of the elasticity theory with a Timoshenko beam assumption discretized by the finite element method in the fixed coordinate system [26]:

$$[M]\{\ddot{w}(t)\} + ([C] + \Omega[G])\{\dot{w}(t)\} + [K]\{w(t)\} = \{F_{ext}\} \quad (6)$$

where $\{w(t)\}^T = \{X(t), Y(t)\}^T$ is the nodal displacement vector; $[M]$, $[C]$, $[G]$, $[K]$ are global mass, damping, gyroscopic,

and stiffness matrices; $\{F_{ext}\}^T = \{F_x, F_y\}^T$ is the external force vector.

The coupled nonlinear system describing the gas film domain in the HGGBs, transient response of the rotor, and interconnection of the forces generated in the bearing film and journal center displacement due to transient rotor vibrations are:

$$\begin{cases} \frac{\partial}{R\partial\theta}\left(\frac{ph^3}{12\mu}\frac{\partial p}{R\partial\theta}\right)+\frac{\partial}{\partial z}\left(\frac{ph^3}{12\mu}\frac{\partial p}{\partial z}\right)=\frac{u}{2}\frac{\partial(ph)}{R\partial\theta}+\frac{\partial(ph)}{\partial t}; \\ h_0 = c_g + c + e\cos(\theta-\Phi); \\ \{f_{HGGB}(t)\}=\begin{Bmatrix} f_x \\ f_y \end{Bmatrix}=-\int_0^{2\pi}\int_0^l \begin{Bmatrix} \Delta p\cos\theta\, R \\ \Delta p\sin\theta\, R \end{Bmatrix} dz d\theta; \\ \{f_{HGGB}(t)\}\rightarrow\{F_{HGGB}(t)\}; \\ [M]\{\ddot{w}(t)\}+([C]+\Omega[G])\{\dot{w}(t)\}+[K]\{w(t)\}= \\ =\{F_{ext}\}+\{F_{HGGB}(t)\}; \\ \{w(t)\}^T\rightarrow e \end{cases} \quad (7)$$

The boundary conditions for the nonlinear system in the gas film domain at all boundaries are:

$$p_0 = 101.325\ kPa. \quad (8)$$

The time integration of the system is based on Newmark's algorithm [26].

3. CASE DESCRIPTION AND SIMULATION MODEL

3.1 Case Description

The considered case of the rotor installed in the herringbone groove journal bearings involves the radial anode off-gas recirculation fan for solid oxide fuel cell systems [27]. The operation of a machine of this type was theoretically and experimentally proven for lubrication of the herringbone groove journal bearings by the air [28] and the vapor [29]. The scheme of the machine is presented in Fig. 1. The arrow in Fig. 1 indicates rotating direction.

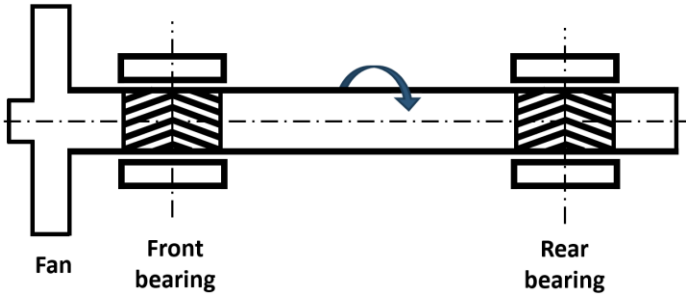

FIGURE 1: ROTOR-HGGJB SYSTEM SCHEME

This machine's nonlinear rotor dynamics was studied comprehensively by several theoretical [30] and experimental investigations [31]. The device is well-described and tested; therefore, it is a sound basis for further exploration in the theoretical field.

Previous studies were performed for the grooved rotor (rotating grooves), but the question of the influence of the groove location either on the rotor or on the journal is still present. Such a study can be performed by applying the FE approach, whereas many authors use narrow groove theory to describe the behavior of herringbone groove bearings.

The current paper studies the rotating vs. stationary grooves phenomenon. It provides a comprehensive comparison of the nonlinear response of the considered rotor in the herringbone groove gas journal bearings with stationary and rotating grooves in terms of their influence on the rotor stability and the rotor motion for different rotational speeds applying detailed simulation of bearings geometry by finite element method.

3.2 Bearing Model

The general approach to bearing modeling is similar to the one described for oil hydrodynamic and hydrostatic bearings [19,20]. The motion of the bearing center is considered in the X and Y coordinates (shown in Fig. 2) referring to the rotor coordinate system, and the Z coordinate coincides with the undeformed rotor axis.

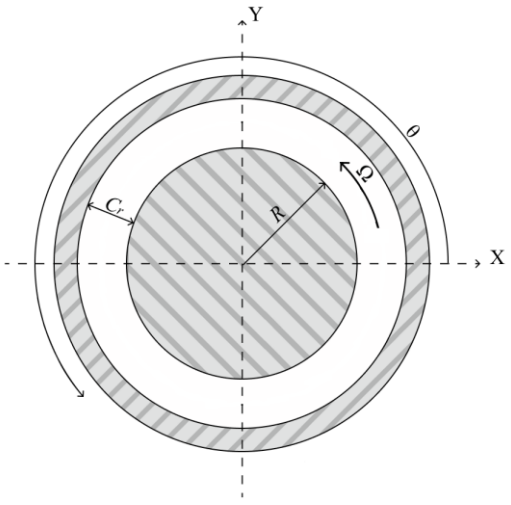

FIGURE 2: BEARING SCHEME AND NOTATION

The Reynolds equations are solved in the circumferential coordinate system with the same axial coordinate Z, averaging by the radial coordinate and with the circumferential coordinate φ starting from the positive X direction, as shown in Fig. 2 (the rotor rotation is counterclockwise).

In contrast to hydrodynamic and hydrostatic bearings, the ideal gas model is used for herringbone groove gas journal bearing modeling. Half of the bearing in the axial direction is considered, and the rest is modeled in symmetric conditions. The bearing fluid film is discretized by finite elements (FE).

The main bearing parameters are taken from the paper [30] and shown in Table 1.

TABLE 1: BEARING PARAMETERS

Parameter	Value	Units
Bearing length	8	mm
Bearing diameter	8	mm
Bearing clearance	8	μm
Groove depth	8	μm
Groove length	4	mm
Groove width	14.625	deg
Groove inclination to the axial line	56.2	deg
Groove count	16	-
Air temperature (average)	220	°C
FE number in the circumferential direction	64	-
FE number in the axial direction	10	-

The table shows that the ratio of the bearing radial clearance to the bearing diameter C_r/D is 0.001. This value is higher than the values available in the classic literature for HGGJBs. For example, the experimental work [15] considers the rotor configurations with the C_r/D ratios from 0.00021 to 0.00042. Such values are typical for gas bearings with herringbone grooves, although smaller values like 0.0001 are also possible. The fact that the bearing provides the rotor with sufficient characteristics with the ratio C_r/D = 0.001 indicates the optimal pattern of herringbone grooves, which generate the required parameters with this ratio being twice as high as the early investigations of HGGJBs [15].

The finite element mesh shown in Fig. 3 was checked to deliver the best acceptable accuracy keeping a reasonable calculation time. The 64 finite elements were selected in the circumferential direction (four elements for each groove-land region: one element modeling the land, one element modeling the maximal groove depth, and two narrow elements with 0.1 of the groove width modeling the clearance change between the land and the groove). The ten finite elements were specified for discretizing half of the bearing in the axial direction.

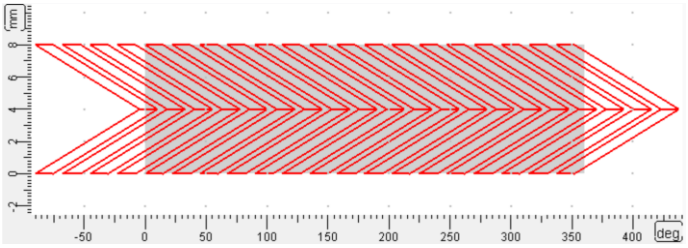

(A)

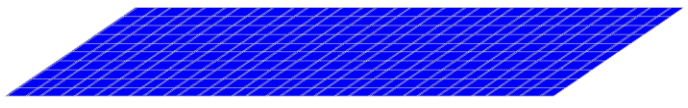

(B)

FIGURE 3: UNWRAPED VIEW OF BEARING GEOMETRY (A) AND FINITE-ELEMENT MESH (B)

The finite element mesh convergence studies were performed for steady-state bearing operation. The criteria for the number of finite elements were as follows: the difference between the calculated results (minimal film thickness, maximal pressure, and flow) for a mesh twice as fine and the current mesh must be less than 2%. This allowed the selection of optimal parameters for the FE grid that provide sufficient accuracy. The distributions of these parameters for one of the considered cases are shown in Fig. 4. The pressure distribution was also observed visually to check the smoothness of the generated field (Fig. 5).

(A)

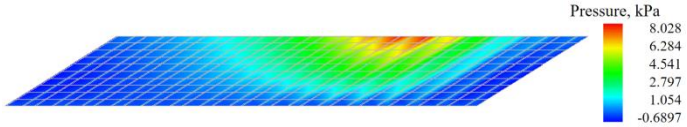

(B)

FIGURE 4: HYDRODYNAMIC PARAMETERS DISTRIBUTIONS FOR THE FRONT BEARING WITH STATIONARY GROOVES AT 10000 RPM: (A) CLEARANCE; (B) PRESSURE

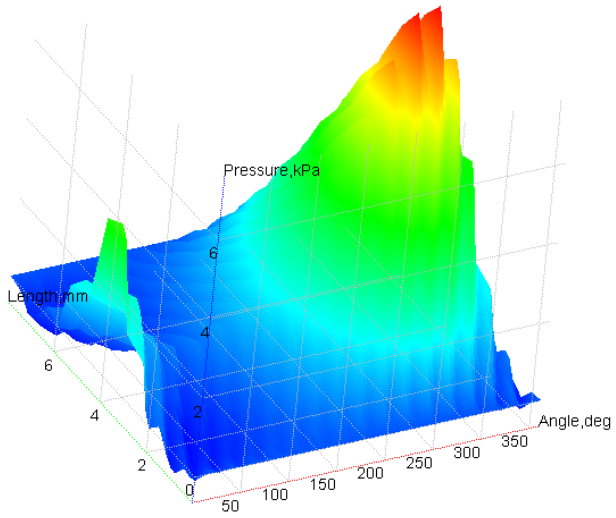

FIGURE 5: BEARING PRESSURE DISTRIBUTION IN THE THREE-DIMENSIONAL VIEW FOR THE FRONT BEARING WITH STATIONARY GROOVES AT 10000 RPM

3.3 Rotor Dynamics Model

The rotor simulation FE model is shown in Fig. 6. The FE model was built using the Timoshenko beam finite elements that

were used for the shaft discretization, and the attached equipment (i.e., fan) is modeled with lumped mass-inertia elements (blue circles in Fig. 6). The left and right sides in the figure correspond to the front and rear bearings respectively. A red arrow in the figure represents the applied unbalance.

The created FE rotor dynamics model corresponds to the parameters presented in the publication [30]. Note that loads acting on the rotor were applied differently than [30]. The residual unbalance value was applied to the impeller (corresponding node), and the full gravity load was applied as a static part. At the same time, the paper [30] considers the unbalance distributed between the bearing locations and the inclined rotor mounting (therefore, a partial value of the gravity load is accounted for).

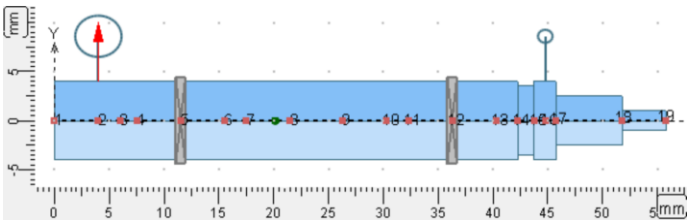

FIGURE 6: ROTOR FINITE-ELEMENT MODEL

Table 2 shows the whole parameter set used in the calculations for the rotor model.

TABLE 2: ROTOR PARAMETERS

Parameter	Value	Units
Rotor length	55.78	mm
Rotor mass	0.0271	kg
Diametral moment of inertia	7.782e-6	kg m^2
Polar moment of inertia	6.07e-7	kg m^2
Bearing span	25.78	mm
Unbalance value	0.01	g mm
Unbalance location	Impeller	-
Gravity acceleration in the Y direction	-9.81	m/s^2
FE number	17	-
FE type	Timoshenko beam	

Before conducting the nonlinear analyses, the rotor's free-free critical speeds were calculated to find the first flexible mode and check if the corresponding critical speed could be in the considered rotational speed range. Fig. 7 shows the free-free Campbell diagram and the first flexible forward whirl mode shape. Neither first backward nor forward whirl critical speeds lie in the rotational speed range between 10000 rpm and 200000 rpm, which is intended to be taken for calculations.

This can also be concluded by observing the critical speed map for the variable bearing stiffness shown in Fig. 8. The only two critical speed lines corresponding to the cylindrical and conic rigid body modes lie in the rotational speed range between 10000 rpm and 200000 rpm. This allows for an expectation of the rigid rotor response during nonlinear rotor dynamics calculations within this rotational speed range.

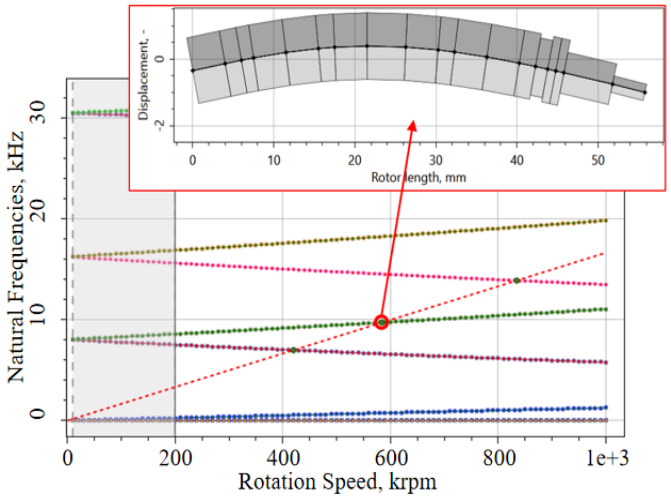

FIGURE 7: FREE-FREE CAMPBELL DIAGRAM AND FREE-FREE FORWARD WHIRL MODE SHAPE CORRESPONDING TO THE FIRST CRITICAL SPEED OF 584045 RPM

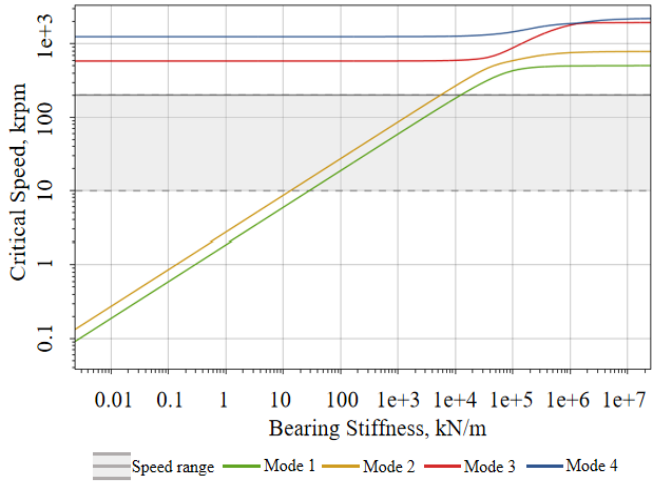

FIGURE 8: CRITICAL SPEED MAP

3.4 Nonlinear Transient Analysis Settings

The nonlinear transient analyses were performed to get the steady rotor response under the unbalance loading and initial excitation in the ramped gravity load application, corresponding to 0.1 of the total simulation time. The settings for analyses are shown in Table 3.

TABLE 3: ANALYSIS SETTINGS

Parameter	Value	Units
Time step amount*	10000	-
Time step value	1e-5	s
Starting rotational speed	10000	rpm
Ending rotational speed	200000	rpm
Time step amount for gravity load ramp	1000	-
Time step amount for unbalance load ramp	0	-

Note for the parameter ‘Time step amount’ from Table 3: convergence studies were performed for finite element meshes and various numbers of transient sub-steps. For some rotational speeds, there was a need to calculate more time steps (50000 and 100000 steps).

Conclusions about the system’s stability were made based on rotor trajectory over time and vibration amplitude analysis. After the transition process takes some time, amplitudes should be less or at least of the same order with bearing clearance and not change over time.

4. RESULTS AND DISCUSSION

The results of the experimental investigation are presented in the work [30] in the form of waterfall diagram plots which indicate the increase of rotor vibrations due to possible instability issues at a sub-synchronous frequency (0.4 multiplicity of the rotor angular velocity), which has the critical impact on the rotor operation for the rotational speed 56 000 rpm. Since these were two obvious integral indicators in the experiment (and no experimental orbit plots were presented), they were chosen to validate the results of the rotating groove case.

The results of the nonlinear transient analysis are presented in paragraphs 4.1 and 4.2 for cases with rotating (grooves on the rotor) and non-rotating (grooves on the bearing shell) domains, respectively.

It should be noted that the rotor mathematical model allows deflections in the bearing locations higher than the bearing radial clearance (eccentricity ratios higher than 1 are mathematically possible). In these cases, the artificial 'springs' are added to avoid infinitesimal deflections. Some of the amplitude plots in the following results can contain amplitudes higher than the bearing clearance due to this fact. However, these cases should be considered a definite instability with the rubbing of a shaft and a bearing shell. The observations of rotor displacements higher than the bearing clearance are unrelated to the physical process.

4.1 Stationary Grooves

The rotor arrangement with stationary grooves (the grooves on the bearing shell) does not correspond to the design of the experimental rig discussed in [30]; however, its consideration is valuable for comparison purposes with the case of the rotating groove. Suppose the results of calculations for the rotating grooves show good correspondence to the experimental data. In that case, this will allow comparing the calculation results for the stationary and rotating groove cases and making conclusions about the benefits of locating the grooves on the bearing shell or the rotor.

Fig. 9 and Fig. 10 represent predicted trajectories of vibrational motion over time and at different rotor speeds, measured at front and rear bearings for the case when the groove pattern is located on the stationary component (bearing), which is non-rotating. The results presented in Fig. 9 correspond to the front bearing, and Fig. 10 corresponds to the rear bearing.

The study indicates that the stable vibrational motion of the system is observed up to the speed of 22 000 rpm. For the speed range of 22 000 – 200 000 rpm, unstable behavior takes place.

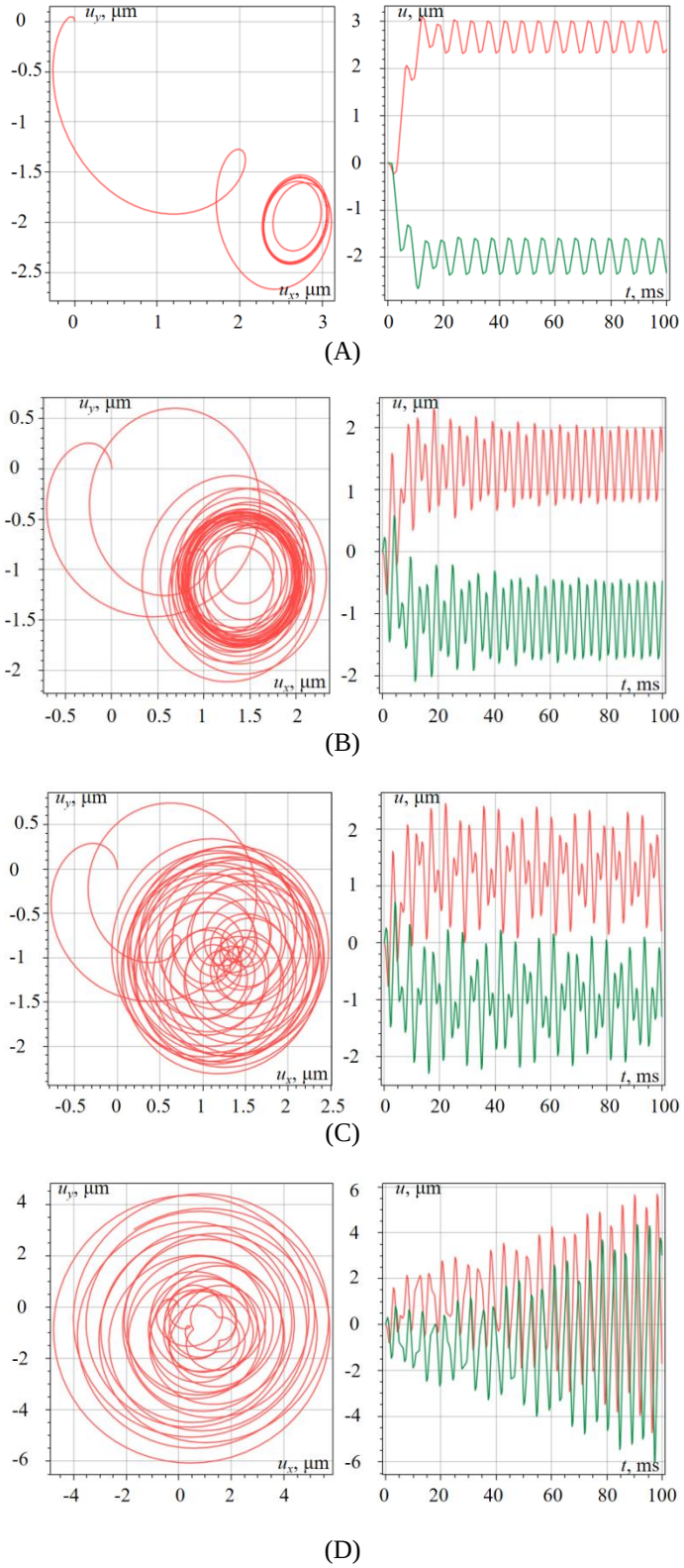

FIGURE 9: PREDICTED TRAJECTORIES FOR THE STATIONARY GROOVE CASE CALCULATED AT DIFFERENT ROTOR SPEEDS FOR THE FRONT BEARING: (A) 10 000 RPM; (B) 20 000 RPM; (C) 22 000 RPM; (D) 24 000 RPM

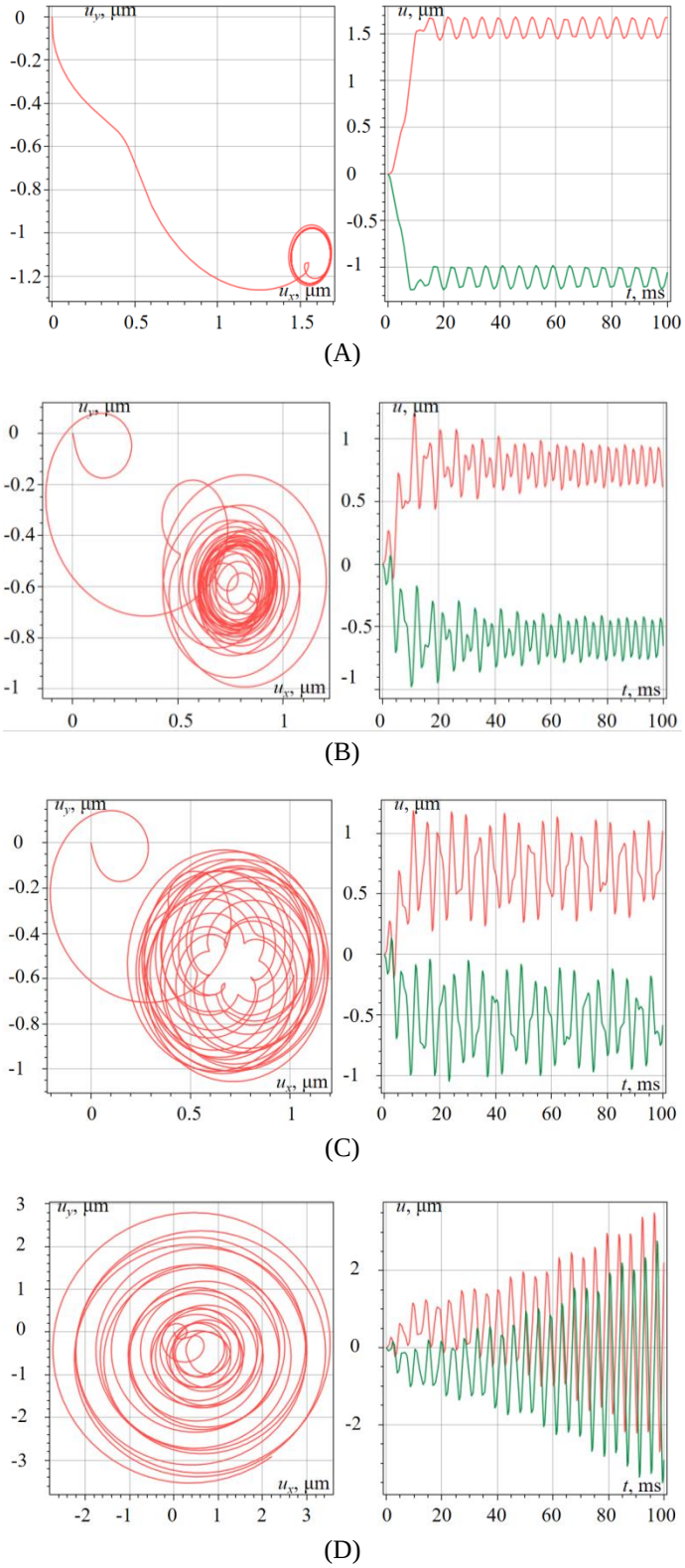

FIGURE 10: PREDICTED TRAJECTORIES FOR THE STATIONARY GROOVE CASE CALCULATED AT DIFFERENT ROTOR SPEEDS FOR THE READ BEARING: (A) 10 000 RPM; (B) 20 000 RPM; (C) 22 000 RPM; (D) 24 000 RPM

The Waterfall plots calculated for the range of 10 000 – 200 000 rpm are presented in Fig. 11 (radial displacements are measured at the front bearing).

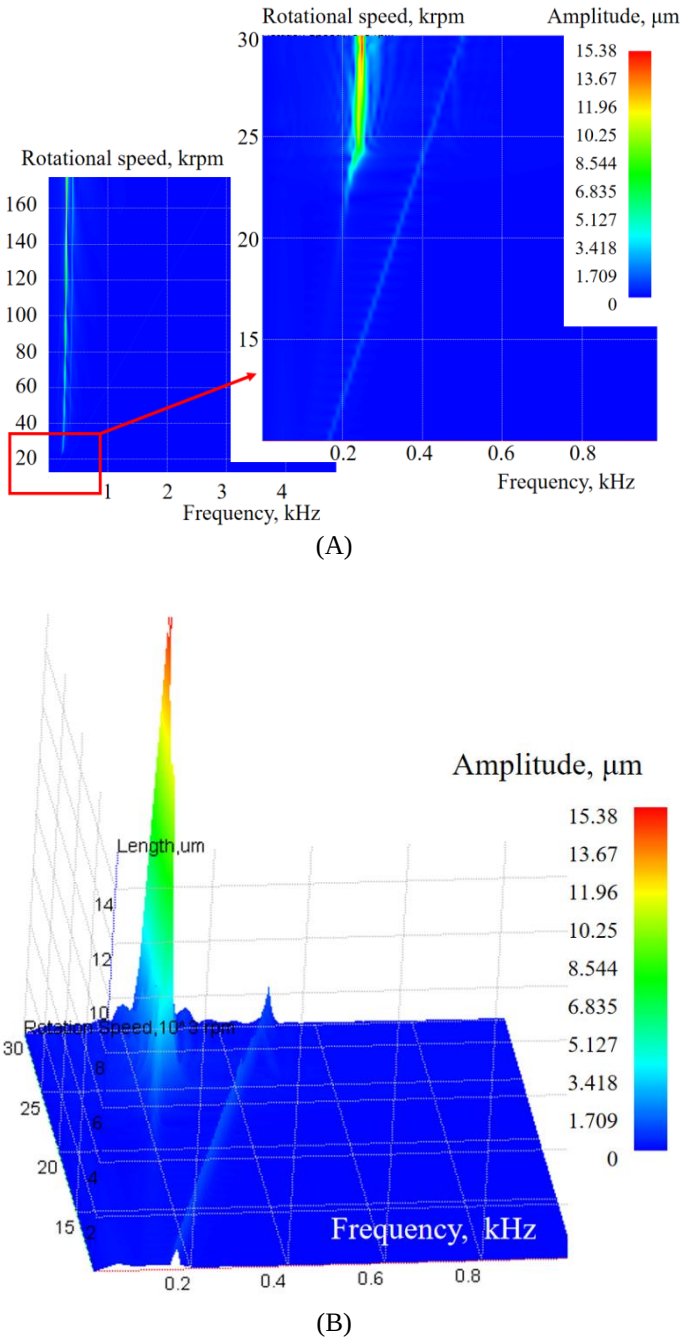

FIGURE 11: WATERFALL PLOTS FOR STATIONARY GROOVE CASE: (A) 2D VIEW; (B) 3D VIEW

A rapid increase in amplitudes is observed at the rotational speed of 22 000. Sub-synchronous vibrations occur at a whirl frequency ratio (ratio between sub-synchronous and rotational frequencies) of ~0.4. The synchronous amplitudes are relatively small (with the applied unbalance value).

The comparison of the results for the stationary groove case with the rotating groove case, which is considered below in this paper, shows a significant difference in stability threshold: unstable motion takes place at a much lower operating speed for the calculated results.

4.2 Rotating Grooves

Nonlinear transient analysis results for the case with rotating grooves are presented in Fig. 12 – 16. Fig. 12 – 15 show calculated trajectories of rotor vibrational motion over time and at different rotation speeds, measured at the front and rear bearings. Fig. 16 represents the Waterfall plot for the case with rotating grooves.

In cases where rotating grooves (on a rotor) are considered, amplitudes grow at 30 000 rpm up to 70 000 rpm, where sub-synchronous vibrations appear. The whirl frequency ratio for the sub-synchronous vibrations detected when rotating grooves were considered is the same as for the stationary groove case (approximately ~0.4). The synchronous amplitudes due to the considered unbalance value are relatively small within the whole range of analysis rotor speed.

The obvious increase of vibrational amplitudes occurs in the range from 40 000 rpm to 70 000 rpm with a sharp peak near 55 000 rpm at 0.4 multiplicity of the rotor angular velocity, which indicates the instability issue and corresponds to the experiment [30] where the instability issue is indicated at 56 000 rpm.

During the experiment, the system was shut down at 56 000 rpm to prevent the further increase of amplitudes, however, the calculations presented below for the rotating groove case indicate that the further growth of the rotational speed will result in the decrease of vibrational amplitudes.

Unlike the results of simulations performed for stationary grooves, which do not correspond to the actual system considered in the experiment but are still valuable for comparison purposes, in the case of rotating grooves, the results are in good agreement with the experiment [30]. This is particularly evident regarding the minimum rotational speed at which the system may lose stability (approximately 55 000 rpm), where the increase in vibrations observed in the experiment can be attributed to the loss of stability. However, another effect has been detected based on the simulation considering rotating grooves: the system became stable again at the rotating speed of ~70 000 rpm up to 190 000 rpm. This is demonstrated in the Waterfall diagram in Fig. 16. Such an effect was not captured in the analysis with stationary grooves (grooves on the bearing shell).

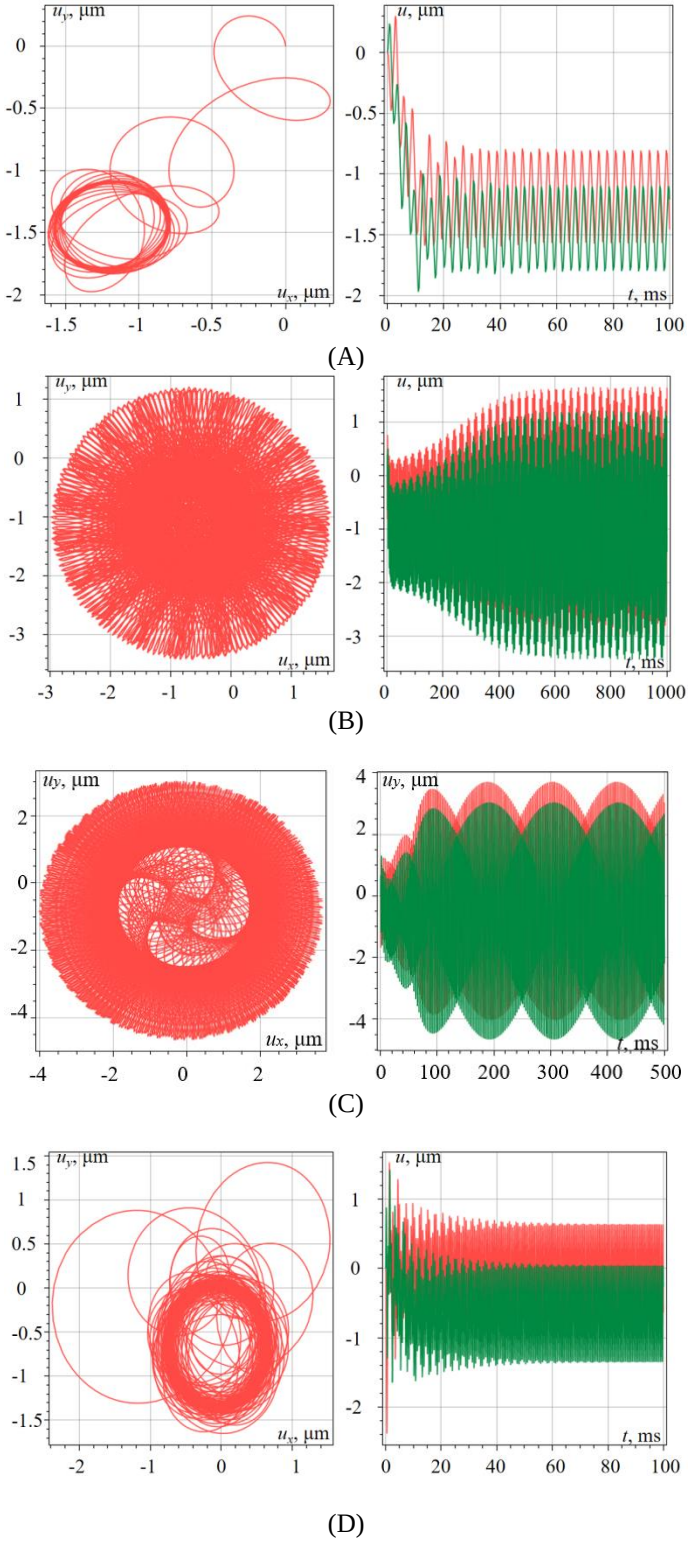

FIGURE 12: PREDICTED TRAJECTORIES FOR THE ROTATING GROOVE CASE CALCULATED AT DIFFERENT ROTOR SPEEDS FOR THE FRONT BEARING: (A) 20 000 RPM; (B) 40 000 RPM; (C) 60 000 RPM; (D) 100 000 RPM

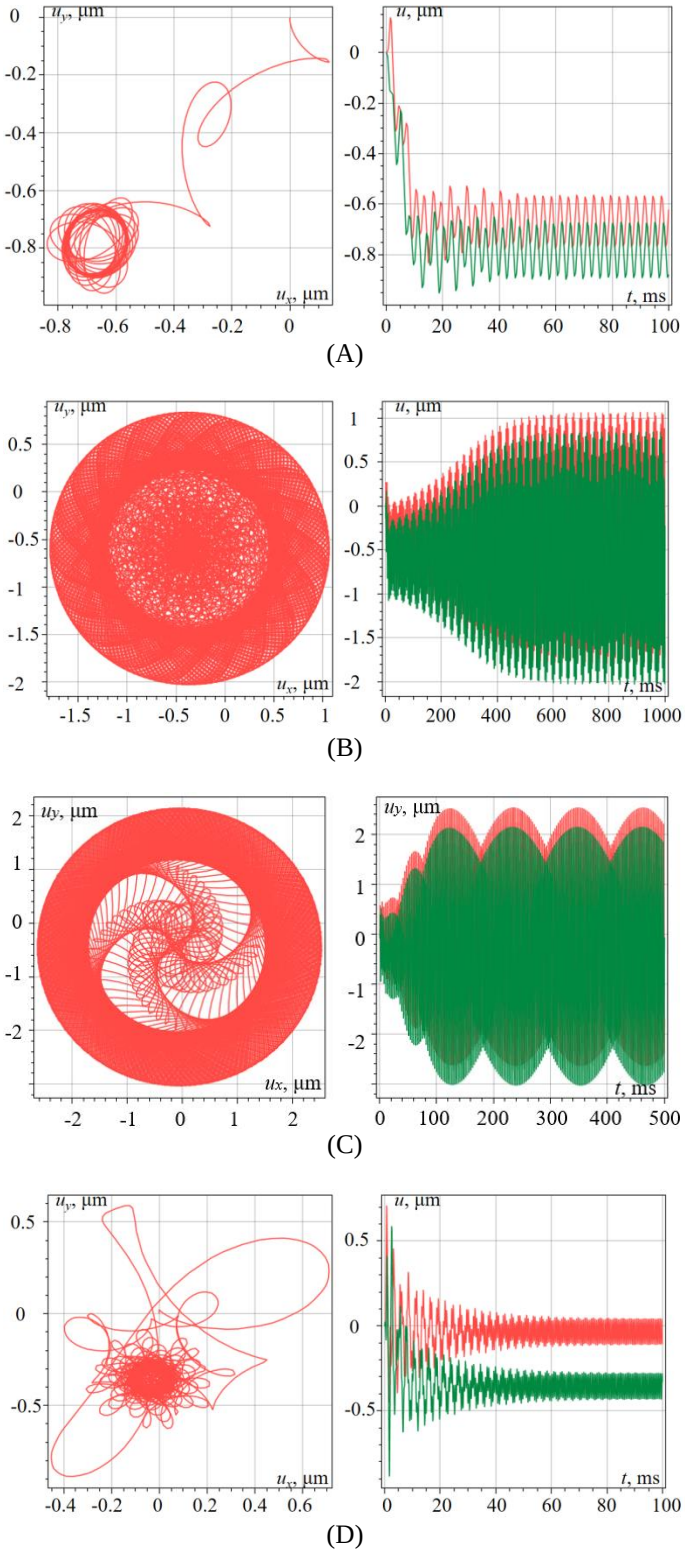

FIGURE 13: PREDICTED TRAJECTORIES FOR THE ROTATING GROOVE CASE CALCULATED AT DIFFERENT ROTOR SPEEDS FOR THE REAR BEARING: (A) 20 000 RPM; (B) 40 000 RPM; (C) 60 000 RPM; (D) 100 000 RPM

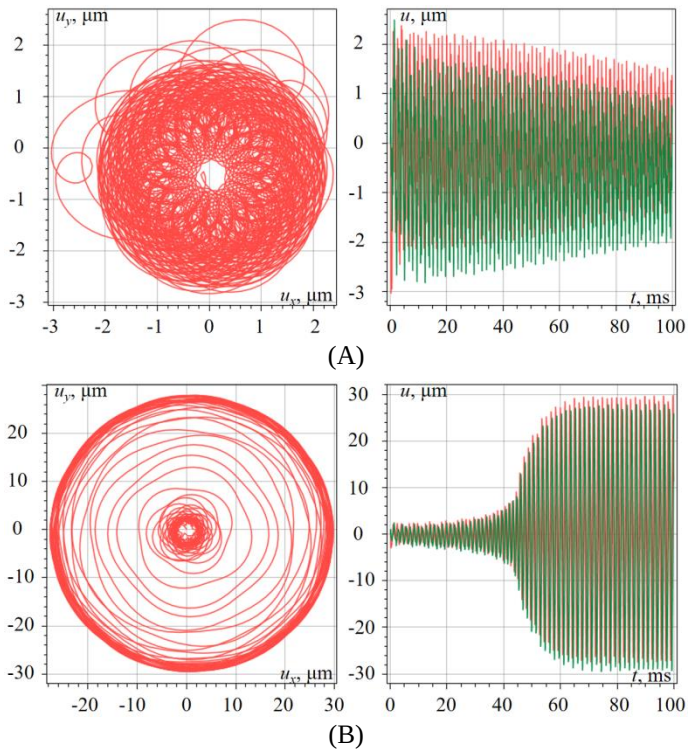

FIGURE 14: PREDICTED TRAJECTORIES FOR THE ROTATING GROOVE CASE CALCULATED AT ROTOR SPEEDS FOR THE FRONT BEARING: (A) 190 000 RPM; (B) 200 000 RPM

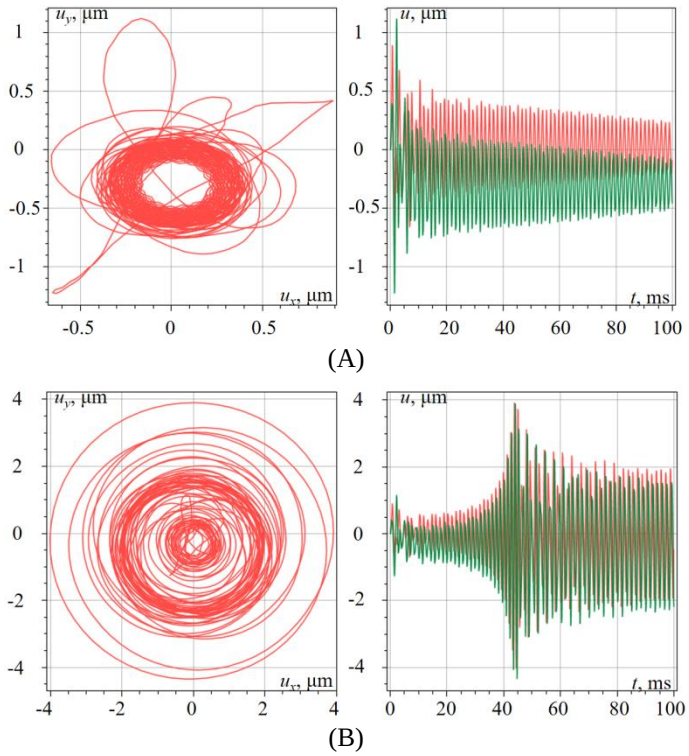

FIGURE 15: PREDICTED TRAJECTORIES FOR THE ROTATING GROOVE CASE CALCULATED AT ROTOR SPEEDS FOR THE REAR BEARING: (A) 190 000 RPM; (B) 200 000 RPM

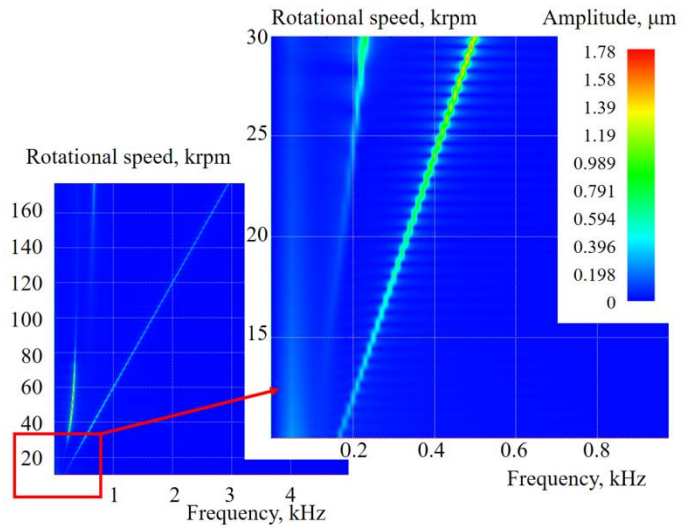

(A)

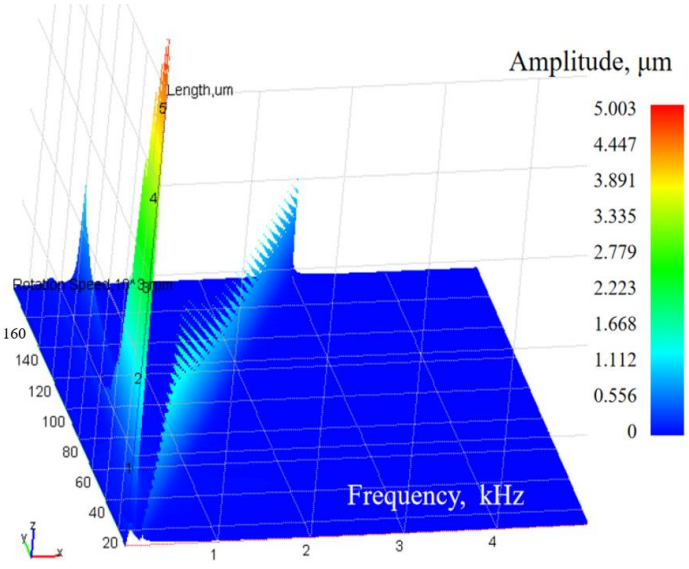

(B)

FIGURE 16: WATERFALL PLOTS OF THE RADIAL DISPLACEMENT (MEASURED AT THE FRONT BEARING), CALCULATED IN THE RANGE OF 10 000 RPM – 200 000 RPM FOR ROTATING GROOVE CASE: (A) 2D VIEW; (B) 3D VIEW

CONCLUSION

An approach to determine the stability of the rotor in herringbone groove gas journal bearings (HGGJB) based on the nonlinear transient analysis has been proposed in this study. The submitted approach allows consideration of rotating (on a rotor) or stationary (on a bearing shell) grooves which is necessary to simulate the physical behavior of the rotor-HGGJB system. Another advantage of the approach is using the FE method, which accurately describes the bearing geometrical model, allows building detailed plots of bearing parameters, and has no limitations even for a small number of grooves of HGGJBs.

An investigation of the nonlinear response and stability for the system of a rotor supported by HGGJBs has been performed for the cases with grooves on stationary components (bearing shells) and with grooves on a rotor (rotating grooves).

It was shown that rotating grooves for rotor-HGGJB application provide much better stability than the case with stationary grooves.

The performed study of the rotor-HGGJB application and comparison between the stationary and rotating groove cases confirms the significant influence of rotating grooves on the stability of the system (and threshold speeds). It was shown that the obtained results are in good agreement with experimental measurements [30] for the case which corresponds to the physical system – when rotating grooves are considered. The predicted region with the increased vibration amplitudes for the rotating groove case is between 40 000 rpm and 70 000 rpm, with a sharp peak at 55 000 rpm that indicates the unstable behavior of the system. This is in agreement with experimental measurements. The considered physical system also obtained an additional effect of decreased vibrations at speeds higher than 70 000 rpm.

These investigations for the rotating groove case indicate that although some instability issues may occur at sub-synchronous frequencies, they can be successfully overcome if the bearing clearance and vibration limits are not violated at the low-speed regions with the increased amplitudes of vibration. These observations are possible due to the careful analysis of orbit plots in the bearing locations for different rotational speeds.

For the stationary groove case though, the vibration amplitudes violate the bearing clearance at low rotational speeds (approximately 22 000 rpm) proving the lower effectiveness of locating the grooves on the bearing shell.

The approach presented in this article is a combination of proven methods and solutions for nonlinear analysis of rotor-HGGJB systems that possess good accuracy and can be used for engineering purposes at the design stage of product development, potentially, for a wide range of HGGJB designs (including designs with a small number of grooves) and operating parameters.

The study shows the importance of nonlinear rotor dynamics calculations in a wide range of rotational speeds, in addition to experimental investigations.

REFERENCES

[1] Whipple, R. T. P., 1958, *The Inclined Groove Bearing*.

[2] Vohr, J. H., and Chow, C. Y., 1965, "Characteristics of Herringbone-Grooved, Gas-Lubricated Journal Bearings," Journal of Basic Engineering, **87**(3), pp. 568–576.

[3] Iseli, E., Guenat, E., Tresch, R., and Schiffmann, J., 2020, "Analysis of Spiral-Grooved Gas Journal Bearings by the Narrow-Groove Theory and the Finite Element Method At Large Eccentricities," J Tribol, **142**(4).

[4] Guenat, E., and Schiffmann, J., 2019, "Multi-Objective Optimization of Grooved Gas Journal Bearings for

Robustness in Manufacturing Tolerances," Tribology Transactions, **62**(6), pp. 1041–1050.

[5] Xu, W., and Yang, J., 2019, "Accuracy Analysis of Narrow Groove Theory for Spiral Grooved Gas Seals: A Comparative Study with Numerical Solution of Reynolds Equation," Proceedings of the Institution of Mechanical Engineers, Part J: Journal of Engineering Tribology, **233**(6), pp. 899–910.

[6] Bonneau, D., and Absi, J., 1994, "Analysis of Aerodynamic Journal Bearings With Small Number of Herringbone Grooves by Finite Element Method," J Tribol, **116**(4), pp. 698–704.

[7] Zirkelback, N., and San Andre´s, L., 1998, "Finite Element Analysis of Herringbone Groove Journal Bearings: A Parametric Study," J Tribol, **120**(2), pp. 234–240.

[8] Wang, C. C., 2007, "Bifurcation Analysis of an Aerodynamic Journal Bearing System Considering the Effect of Stationary Herringbone Grooves," Chaos Solitons Fractals, **33**(5), pp. 1532–1545.

[9] Chang, B. H., Chen, P. H., and Lee, D. S., 2012, "Experimental Stability Study on Herringbone-Microgrooved Journal Bearing in an Impeller-Spindle," Journal of Mechanics, **28**(1), pp. 123–133.

[10] Jang, G. H., and Yoon, J. W., 2003, "Stability Analysis of a Hydrodynamic Journal Bearing with Rotating Herringbone Grooves," J Tribol, **125**(2), pp. 291–300.

[11] Song, L., Yuan, G., Zhang, H., Ding, Y., and Cheng, K., 2022, "The Stability of Spiral-Grooved Air Journal Bearings in Ultrahigh Speeds," Materials, **15**(5).

[12] Miyanaga, N., and Tomioka, J., 2015, "Stability Analysis of Herringbone-Grooved Aerodynamic Journal Bearings for Ultra High-Speed Rotations," International Journal of Materials, Mechanics and Manufacturing, **4**(3), pp. 156–161.

[13] Fleming D.P., and Hamrock B.J, 1974, *Optimization of Self-Acting Herringbone Journal Bearings for Maximum Stability*, Cleveland, Ohio, U.S.A.

[14] Cunningham, R. E., Fleming, D. P., and Anderson, W. J., 1969, "Experimental Stability Studies of the Herringbone-Grooved Gas-Lubricated Journal Bearing," Journal of Lubrication Technology, **91**(1), pp. 52–57.

[15] Cunningham, R. E., Fleming, D. P., and Anderson, W. J., 1971, "Experimental Load Capacity and Power Loss of Herringbone Grooved Gas Lubricated Journal Bearings," Journal of Lubrication Technology, **93**(3), pp. 415–422.

[16] Liu, X., and Chen, W., 2022, "Structural Design and Optimization of Herringbone Grooved Journal Bearings Considering Turbulent," Applied Sciences (Switzerland), **12**(1).

[17] Gad, A. M., Nemat-Alla, M. M., Khalil, A. A., and Nasr, A. M., 2006, "On the Optimum Groove Geometry for Herringbone Grooved Journal Bearings," J Tribol, **128**(3), pp. 585–593.

[18] Schlums, H., Hühne, C., and Sinapius, M., 2022, "Design of a Herringbone-Grooved Bearing for Application in an Electrically Driven Air Compressor," Machines, **10**(8).

[19] Moroz, L., Romanenko, L., Kochurov, R., and Kashtanov, E., 2018, "Hydrodynamic Journal Bearings Optimization Considering Rotor Dynamics Restrictions," *Volume 7B: Structures and Dynamics*, American Society of Mechanical Engineers.

[20] Moroz, L., Romanenko, L., Kochurov, R., and Kashtanov, E., 2020, "Load Influence on Hydrostatic Oil Film Journal Bearing Stiffness Characteristics," *Volume 10A: Structures and Dynamics*, American Society of Mechanical Engineers.

[21] Martynenko, V., 2020, "Analysis of Strength and Bearing Capacity of the Auxiliary Mine Ventilation Fan Connected to the Rotor of Its Electrical Drive," *2020 IEEE KhPI Week on Advanced Technology (KhPIWeek)*, IEEE, pp. 19–23.

[22] Martynenko, G., and Martynenko, V., 2020, "Rotor Dynamics Modeling for Compressor and Generator of the Energy Gas Turbine Unit with Active Magnetic Bearings in Operating Modes," *2020 IEEE Problems of Automated Electrodrive. Theory and Practice (PAEP)*, IEEE, pp. 1–4.

[23] Martynenko, G., 2020, "Analytical Method of the Analysis of Electromagnetic Circuits of Active Magnetic Bearings for Searching Energy and Forces Taking into Account Control Law," *2020 IEEE KhPI Week on Advanced Technology (KhPIWeek)*, IEEE, pp. 86–91.

[24] Chu, L.-M., Li, W.-L., Shen, R.-W., and Tsai, T.-I., 2009, "Dynamic Characteristics of Grooved Air Bearings in Microsystems," Proceedings of the Institution of Mechanical Engineers, Part J: Journal of Engineering Tribology, **223**(6), pp. 895–908.

[25] Hamrock, B. J., Schmid, S. R., and Jacobson, B. O., 2004, *Fundamentals of Fluid Film Lubrication*, CRC Press.

[26] Vollan, A., and Komzsik, L., 2012, *Computational Techniques of Rotor Dynamics with the Finite Element Method*, CRC Press.

[27] Wagner, P. H., Wuillemin, Z., Diethelm, S., van Herle, J., and Schiffmann, J., 2017, "Modeling and Designing of a Radial Anode Off-Gas Recirculation Fan for Solid Oxide Fuel Cell Systems," Journal of Electrochemical Energy Conversion and Storage, **14**(1).

[28] Wagner, P. H., van herle, J., and Schiffmann, J., 2020, "Theoretical and Experimental Investigation of a Small-Scale, High-Speed, and Oil-Free Radial Anode Off-Gas Recirculation Fan for Solid Oxide Fuel Cell Systems," J Eng Gas Turbine Power, **142**(4).

[29] Wagner, P. H., Wuillemin, Z., Constantin, D., Diethelm, S., van herle, J., and Schiffmann, J., 2020, "Experimental Characterization of a Solid Oxide Fuel Cell Coupled to a Steam-Driven Micro Anode off-Gas Recirculation Fan," Appl Energy, **262**.

[30] Liu, W., Bättig, P., Wagner, P. H., and Schiffmann, J., 2020, “Nonlinear Study on a Rigid Rotor Supported by Herringbone Grooved Gas Bearings: Theory and Validation,” Mech Syst Signal Process, **146**.

[31] Bättig, P. K., Wagner, P. H., and Schiffmann, J. A., 2022, “Experimental Investigation of Enhanced Grooves for Herringbone Grooved Journal Bearings,” J Tribol, **144**(9).